Integrated Dielectrophoretic and Impedimetric Biosensor Provides a Template for Universal Biomarker Sensing in Clinical Samples

Logeeshan Velmanickam[1], Vidura Jayasooriya[1], and †Dharmakeerthi Nawarathna[1,2]

Department of Electrical and Computer Engineering[1], Biomedical Engineering Program[2]

North Dakota State University, Fargo, ND.

† Corresponding author

Abstract:

The detection and quantification of nucleic acid and proteomic biomarkers in bodily fluids is a critical part of many medical screening and diagnoses. However, majority of the current detection platforms are not ideal for routine, rapid and low-cost testing in point-of-care settings. To address this issue, we developed a concept for a disposable universal point-of-care biosensor that can detect and quantify nucleic acid and proteomic biomarkers in diluted serum samples. The central tenet of sensing is the use of dielectrophoresis, electrothermal effects and thermophoresis to selectively and rapidly isolate the biomarkers of interest in electrodes and then quantify using electrical impedance. When the sensor was applied to quantify microRNA and antigen biomarker molecules directly in diluted serum samples, it produced a limit of detection values in the fM range and sensitivity values from 10^{12} to 10^{15} Ω/M with a 30-min assay time and assay cost of less than $50 per assay.

1. Introduction

Circulating biomarker testing is a commonly used screening and diagnosis method for diseases such as cancer, cardiovascular disease, and infections [1-3]. Nucleic acid (e.g., DNA, microRNA (miRNA)) and/or protein (e.g., antigen) biomarker molecules are common targets found in bodily fluids (e.g., blood or serum).[1-6] Currently, detection of these biomarkers utilizes multiple assays and instruments dedicated to each type of molecules. For example, expression profiling of nucleic acid biomarkers is commonly performed using quantitative polymerase chain reaction (qPCR).[7-8] In addition, next-generation sequencing (NGS)-, microarray-, electrochemical-, plasmonic-, and hybridization-based nucleic-acid sensors have also been utilized to a lesser degree.[9,10] The enzyme-linked immunosorbent assay (ELISA) is used for antigen expression profiling.[11] In addition, lateral flow immunoassays (LFIA) are also used in the antigen detection[12]. The suitability and applicability of these biomarker detection methods for routine biomarker testing in point-of-care settings is questionable because they are semi-quantitative, complex and multi step assays, time consuming, costly, and need trained staff and expensive equipment.

The miniaturized devices have been revolutionizing many areas of biology, biomedical engineering and clinical research[13]. Miniaturization provides excellent avenues for increasing the performance, reduction the assay cost and time. Therefore, miniaturized devices are attractive to point-of-care applications. For example, dielectrophoresis and magnetophoresis based miniaturized devices have been successfully utilized to quickly manipulate, separate, concentrate and detect clinically important biological cells (e.g., circulating tumor cells) [13]. In addition, low-cost miniaturized devices were also developed to detect and quantify nucleic acid and antigen molecules. Majority of these sensing devices utilize qPCR and ELISA assays to detect/quantify nucleic acid or antigen biomarkers[14-15]. Therefore, all most all-technical issues (e.g., low sensitivity, high cost) associated with qPCR and ELISA were inherited to these devices. One potential avenue to address this issue is to investigate a viable point-of-care sensing concept that is outside qPCR and ELISA. In this work, we have developed a template for miniaturized universal biosensor that can detect and quantify both nucleic acid and antigen biomarkers. Below, we discussed the basic concept of the universal biomarker-sensing device and underlying physics of sensing. Finally, to demonstrate the proof-of-concept of concept, we applied the device

to quantify spiked miRNA and antigen molecules in diluted serum samples. Both miRNA and antigen molecules are commonly used biomarkers for many diseases.

The universal biomarker detection and quantification assay has three steps; step (1) was performed in a commercially available micro-centrifuge tube, and the other steps (step 2 and 3) were performed on the disposable device that we developed for this study (Figure 1(a)). Traditional finger-like interdigitated electrodes have been used in a number of biomedical assays, including cell separation, cell detection, and molecular analysis assays.[16-20] However, in this study, we designed T-shaped interdigitated electrodes (TIEs) that are consisting of semi-circular and straight rectangular electrodes (Figure 1(b)) to efficiently separate and concentrate target biomarker molecules. T-section of the TIEs are hotspots of high electric field and temperature gradients that were utilized to separate and concentrate target biomarker molecules.

In step (1), target biomarker molecules of interest were conjugated/hybridized with their complementary molecules. For example, to analyze the expression of miRNA molecules that are typically about 22 nucleotides (nt) long, DNA molecules (22 nt) that were complementary to the target miRNA were added to the sample (e.g., serum) and hybridized with the target miRNA to produce miRNA-DNA duplex molecules. Similarly, to detect and quantify the expression of antigen molecules, complementary monoclonal antibody molecules were added to the sample and conjugated with target antigens.

In Step 2, separation of the labeled target molecules from non-target molecules were performed and subsequently, target molecules were concentrated in T-section of the TIEs. Speedy separation of target molecules from other molecules with high accuracy is generally difficult to achieve and several methods and devices have been investigated for this purpose; however, these methods require complicated multistep assays that take hours to days to complete, as well as skilled technical personnel, and therefore they are not suited to clinical settings.[21-22] In this study, we developed an approach that uses multiple molecular-field (electric and temperature) interactions to efficiently separate target molecules from other molecules in the sample and selectively concentrate labeled target molecules (e.g., miRNA-DNA duplex molecules) between T-section (or semi-circular and rectangle part). The external AC potentials applied on the TIEs produce temperature and electric fields with their gradients that have maximum values near the TIE electrodes. The

molecular interactions with temperatures, electric fields and their gradients produce electrothermal effects (or electrothermal flow), thermophoresis and dielectrophoresis. The extent (magnitude and direction) of those effects could depend on the molecular structure of the affected molecules (e.g., conjugated vs. not conjugated and single-stranded vs. double-stranded).[23] We have utilized these interactions to separate the conjugated molecules (or target molecules) from other molecules (non-target molecules) and concentrate them on the TIEs.

In step (3), the concentrated target molecules in the TIEs were quantified. There are multiple methods available for molecular quantification. For example, fluorescence-based methods are very popular and widely used for detecting molecules.[24] Detection of molecules with fluorescence requires that target molecules be labeled with fluorophores and fluorescence intensity is used to quantify the biomarker molecules. Since the concentrations of target biomarker molecules are typically minute (< 1 pM) in clinical samples, in fluorescence-based quantification methods, the fluorescence intensity is generally weak and it is therefore difficult to differentiate between the fluorescence intensity of the target biomolecules and the background level of fluorescence. To address this issue, in this work, we investigated the use of electrical impedance. [25-26] Moreover, we have investigated the use of electrical impedance to quantify the target molecules concentrated in TIEs.

Materials and Methods

Device fabrication: The device has planar gold microelectrodes that were manufactured on a commercially available glass substrate via traditional photolithography-based micro-fabrication techniques and details can be found elsewhere.[17] The current version of the device has about 2500 pairs of T-shaped interdigitated electrodes (TIEs; ~100 nm in height) covering a 5 mm × 5 mm area.

Labeling miRNA and antigen molecules with complementary molecules: The hybridization of miRNA and DNA was done at 50℃ and hybridization time of about 10 min were required to label all the target miRNA

molecules.[27] Similarly, to conjugate antigen molecules with complementary monoclonal antibody molecules, molecules were added (antigen and antibody) and incubated at room temperature for about 20-30 min. [28]

COMSOL simulations: AC/DC module was used. Briefly, electrodes were draws to scale, and electric fields, field gradients ($\nabla|E^2|$) and capture regions were calculated. Capture region is the region near the electrodes that satisfies

$$\frac{\frac{1}{2}\alpha E^2}{kT} > 1,$$

where E is the electric field, α is the frequency-dependent electric polarizability of the molecule, k is the Boltzmann constant, and T is the temperature. [27] These calculations were performed by applying an electric potential of 10 Vpp (1 MHz frequency) and assuming that the molecules were suspended in the 0.01x TE buffer (Tris EDTA; 5 μS/cm). α for the miRNA-DNA duplex and free DNA/miRNA in the high frequency (1–50 MHz) condition were 10^{-32} and 3.4×10^{-35} $CV^{-1}m^{-2}$, respectively. [29] We used the Joule heating module and calculated the temperature (T), temperature gradient ($\nabla(T)$) and time-dependent temperature increase near the TIEs. Briefly, in calculations, electrodes were drawn to scale and applied the potential values to the electrodes and calculated the temperature (T), ($\nabla(T)$) and ($E^2\nabla T$) near electrodes.

miRNA and antigen targets: We have selected commercially synthesized MIRLET7 (let-7b; Midland Certified Reagent Company at Midland, TX) miRNA and interleukin-6 (IL-6; BioLegend, San Diego, CA) antigen molecules for detection experiments, as there are biomarkers for number of diseases.[30-31] We used fluorophore-labeled (fluorescein: excitation, 494 nm; emission, 512 nm) nucleic acid (miRNA-DNA and DNA) and protein (antigen-antibody and antibody) molecules in these experiments for easy visualization.

Fluorophore labeled miRNA and antigen detection: Experiments were performed separately for target (e.g., miRNA-DNA) and non-target molecules (e.g., complementary DNA). Briefly, in the experiments, we pipetted 1-μM solutions of target or non-target molecules suspended in 0.01x TE buffer and pipetted about 10 μL of the molecule solutions on TIEs, turned on the electric potential (10 Vpp; 0–10 MHz), waited about 10 min to

achieve the maximum fluorescence intensity, and measured the intensity between TIEs at each frequency. Similarly, antigen and antibody molecules were suspended in 0.01x phosphate-buffered saline (PBS) solution and the rest of the experimental procedure was similar to that of the previous nucleic acid experiment.

Impedance experiments: Commercially available impedance analyzer (Gamry 600, Warminster, PA) was used in the experiments. After concentrating target molecules near TIEs, total impedance and phase spectroscopy of the sample were recorded by applying an electric potential of 10 mV (0–1 MHz). We then plotted the variation of the total impedance and phase angle of the impedance against the frequency for each molecular type.

miRNA detection in .01XTE buffer: We spiked let-7b miRNAs of known molarities to 0.01XTE buffer, hybridized let-7b miRNA with complementary DNA molecules, pipetted about 10 µL of sample onto the device, applied an electric potential of 10 Vpp at 1 MHz, waited about 10 min and measured the total impedance with frequency.

miRNA and antigen detection in serum samples: We have separately spiked commercially available serum samples (Innovative Research, Novi, MI), which were diluted to 1/100 and 1/1000 dilutions, with different let-7b miRNA molarities (0–1 nM). We then hybridized let-7b with complementary DNA molecules (1 ng). About 10 µL of sample was pipetted onto the TIE electrodes, and molecules were separated and concentrated let-7b miRNA-DNA duplex molecules between TIEs (10Vpp, 1MHz for 10 min). We then measured the electrical impedance and the phase at each frequency with the molarities of the samples spiked with let -7b miRNA. Similar procedure was used to quantify IL-6 antigens. Briefly, first, antibody and antigen molecules were mixed at the ratio of 10:1. The mixture was briefly mixed by vortexing, and the sample was kept in the ultra-rocker at room temperature for about 20 min. The sample was then added to the 1/100 or 1/1000 diluted serum samples. About 10 µL of sample was pipetted onto the TIE electrodes, separated and concentrated antigen-antibody molecules between TIEs. The total impedance of the samples was measured. Finally, LOD and sensitivity values were calculated.

Results and Discussion

We have used miRNA detection as a model to demonstrate the molecular separation and concentration using electric field and temperature. First, we theoretically investigated the use of dielectrophoretic force to separate labeled target molecules (e.g., miRNA-DNA) from other molecules (e.g., free DNA, miRNA) in the entire sample volume and concentrate the target molecules in the TIEs. We calculated the expected capture region for labeled biomarker molecules (miRNA-DNA duplex molecules) and single-stranded molecules (free DNA and miRNA). The capture region is the volume near TIEs, where the electric field effectively captures the molecules by dielectrophoresis. [27]

Figure 1(a) shows a picture of the device. Rectangle with yellow colored broken lines shows the detection area. Figure 1(b) show the scanning electron microcopy image of TIEs. Figure 1(c) and (d) show the calculated capture regions in the frequency of 1 MHz for labeled biomarker molecules (miRNA-DNA) and other molecules (DNA and miRNA), respectively. The calculation show that miRNA-DNA molecules have a half spherical capture region that has an approximate diameter of 5 μm and single-stranded miRNA/DNA molecules have a smaller capture region that has a diameter value of about 10 nm or less. According to this calculation, miRNA-DNA molecules that are located within about 5 μm of the electrodes could experience the effects of the applied electric fields or the dielectrophoresis, and similarly, single-stranded molecules that are located within 10 nm or less of the electrodes could experience the dielectrophoretic effects. This is an issue because dielectrophoretic force could be used to concentrate molecules from a very small volume of the sample; this might provide inaccurate results about the total quantity of target molecules or even produce significant variations between runs.

The thermophoretic mobility is a result of thermophoresis, which drives molecules along temperature gradient ($\nabla(T)$), either to the largest or smallest $\nabla(T)$. A temperature distribution or $\nabla(T)$ can be established by applying a voltage to the electrodes. Braun's group recently demonstrated that thermophoresis drives short nucleic acid molecules, such as miRNA-DNA and DNA, along $\nabla(T)$ and concentrates both target (miRNA-DNA) and non-target (complementary DNA) molecules in the location with the highest $\nabla(T)$. [32] In addition, Morgan's group has demonstrated that when non-uniform electric fields and $\nabla(T)$ produce a body force called electrothermal force

(F_E) on the buffer and subsequently produce electrothermal flow.[33-34] Suspended molecules in the buffer experience electrothermal drag force and flow with the buffer. The electrothermal flow has been utilized to flow beads and biomolecules in microfluidics devices. [33-34] The magnitude of the electrothermal drag force is proportional to $E^2\nabla(T)$, where E is the electric field. The exact magnitude of the force is dependent on whether the frequency of the applied electric field is below or above the characteristic frequency (ω_0) of the electrothermal process. Typically, $\omega_0 = \frac{\sigma}{\varepsilon}$, where σ and ε are conductivity and dielectric constant of the buffer, respectively. The use of electric field and temperature (by Joule heating) are attractive to point-of-care applications because they can be produced with external AC potentials. Furthermore, there are no complicated steps or pumps or complex instrumentation associated with these methods. To understand how these phenomena could be used for molecular concentrating near electrodes, we have developed series of COMSOL calculations.

First, we studied the temperature produced by the electrodes (Figure 2(a)). We found that an electric potential of 10 Vpp (1–20 MHz) applied on TIEs produces a maximum temperature increase of about 9–10°C in the 0.01x TE buffer (conductivity = 5 μS/cm). We verified these temperature values by manually recording the temperatures. This temperature increase does not cause any structural damage to the molecules, such as the melting of miRNA-DNA duplex molecules or antigen-antibody conjugates. The electrothermal effects on molecules are weak in this low conductivity buffer. Fuhr et al., have shown the electrothermal pumping at about 90 μS/cm, which is one of the lowest conductivities reported for electrothermal effects.[35] Temperature calculation demonstrates that there is $\nabla(T)$ extending to more than few millimeters from the electrodes in the early stage (time < 5 min; Figure 2(a)). Therefore, thermophoretic effects or thermophoretic mobility concentrate molecules near the electrodes in early stage (time < 5 min).

As the buffer temperature increases (time > 5min), some of the sample buffer evaporates and the volume is drastically decreased (Figure 2(a)). We have found that initial volume of the buffer was reduced by more than 100-fold within 10 min after turning on the potential. The gradual evaporation of buffer increases the conductivity value of the remaining buffer by about 100 times (conductivity~ 500 μS/cm). The increase of buffer conductivity contributes to strong electrothermal drag force and weak dielectrophoretic force on molecules. [33, 36] When time> 5 min, electrothermal and dielectrophoretic effects could also provide contributions to molecular

concentration. Electrothermal and thermophoretic effects are proportional to E^4 and E^2, respectively. Therefore, molecules located near TIEs experience a stronger electrothermal drag velocity than the thermophoretic mobility. In addition, if molecules are located in their corresponding capture regions $\left(\frac{1}{2}\alpha E^2 > kT\right)$, dielectrophoresis is stronger than thermophoresis. Moreover, when time> 5 min, we believe that thermophoresis will be weaker than electrothermal and dielectrophoretic effects.

Next, to study the molecular concentration on the electrode plane (time> 5 min), we calculated the variation of $\nabla(T)$, $\nabla|E^2|$ and $E^2\nabla T$ on the x, y, and z = 0 plane of the TIEs (Figure 2(b, c and d), respectively). As noted earlier, due the increase in conductivity value (500 µS/cm or more), the ω_0 of the electrothermal process is about 10 MHz. When applied frequency of the electric field is less than 10 MHz ($F_E = -0.022\varepsilon E^2\nabla T$), the electrothermal drag force of a molecule is proportional to $-E^2\nabla T$, which means that electrothermal drag force drive the molecules out of the electrodes. [37] However, it could only drive the non-target molecules (e.g., miRNA and DNA) out of the electrodes because target molecules (e.g., miRNA-DNA) are firmly held by a stronger dielectrophoretic force $\left(F_{DEP} = \frac{1}{2}\alpha\nabla|E^2|\right)$. [27] We calculated the approximate maximum dielectrophoretic and electrothermal drag forces on miRNA-DNA molecules near electrodes to be 5×10^{-19} N and 8×10^{-22} N, respectively.

We also found that the smallest dielectrophoretic force of the miRNA-DNA molecules is about 1000 times larger than the maximum dielectrophoretic force of the miRNA and DNA molecules. Therefore, miRNA and DNA will not be captured. These forces are expected produce on molecules that are located in the capture region of miRNA-DNA. We used the $\nabla(T)$, $\nabla|E^2|$ and $E^2\nabla T$ values calculated in Figure 2(b, c, and d) to perform the above calculation. The molecules located outside capture region of miRNA-DNA will be brought to the capture region by thermophoretic mobility but some of these molecules will be repelled by weak electrothermal drag force. The mechanism underlying the molecular separation would be, first, thermophoretic mobility of molecules (miRNA-DNA, DNA and miRNA) drives them toward the electrodes, second, some molecules repel by electrothermal drag force, and finally, once the molecules reach the capture region (5 µm diameter) the dielectrophoretic force concentrates them in TIEs. Very few miRNA and DNA molecules reach their capture volume (10 nm) and therefore only few non-target molecules will be captured.

This analysis agrees with our previous experimental findings, where we used electric fields (10 Vpp at 1 MHz) and analyzed variation of fluorescence intensity near electrodes with time for fluorophore labeled miRNA-DNA and DNA molecules. We found an increase in the fluorescence intensity of fluorophore-labeled miRNA-DNA and DNA molecules for about 4-5 min (thermophoretic effect) and gradually decrease for next 5-9 min (electrothermal viscous drag force> dielectrophoretic force) and significant increases about 10 min only for miRNA-DNA molecules (dielectrophoretic force> electrothermal viscous drag force). [27] These processes combinedly contribute to the performance of the sensor (e.g., sensitivity, specificity and detection limit).

To further investigate the utility of the described molecular separation to separate and concentrate (near TIEs), we have used fluorophore labeled miRNA-DNA, miRNA/DNA, conjugated antigen-antibody and antigen molecules. The dipole moments of nucleic acid and protein (antigen) molecules are significantly larger (more than 100 times) than those of fluorophore molecules. [38] Therefore, the labeling of biomolecules with fluorophore molecules does not have any effect on the biomolecules' dielectrophoretic force. We varied the frequency of the electric potential (0–10 MHz) to determine the best frequency for concentrating and quantifying the nucleic acid and protein molecules.

Figure 3 (a) and (b) show the total fluorescence intensities measured between each TIE vs. frequency of the applied potential for let-7b-miRNA-DNA complexes, DNA that is complementary to let-7b, conjugated IL-6-antigen-antibody complexes, and monoclonal antibody for IL-6, respectively. By closely examining the fluorescence intensity values of Figures 3(a and b), at 1 MHz, miRNA-DNA duplex molecules could be separated and concentrated between TIEs with very high specificity (~100%) or without contamination with single-stranded DNA, and conjugated antigen-antibody complexes could be separated and concentrated with ~100% specificity at 0.6 MHz. Figure 3(c, d, e, f) show the concentration of fluorophore labeled conjugated IL-6 antigen-antibody molecules (10 Vpp at 625 kHz), complementary DNA to let 7b (10 Vpp at 1 MHz), IL-6 antibody (10 Vpp at 625 kHz) and hybridized let 7b-miRNA-DNA (10 Vpp at 1MHz)in TIEs. To locate the place that concentrates the non-target molecules (e.g., complementary DNA and the antibody for IL-6), we measured

the fluorescence intensity on TIEs and saw no accumulation of fluorescence on the electrode (data not shown). We believe that non-target molecules are spread out on TIEs.

As our next step, we studied the potential use of electrical impedance to quantify the molarities of the target biomarkers that are concentrated between TIEs. When the electrical impedance of the TIE array is measured after molecular separation and concentration, it could still measure the cumulative impedance from the target and non-target molecules, metal electrodes, and buffer solution.[26] We developed experiments to understand how the target and non-target molecules that are concentrated in two places in TIEs contribute to the measured electrical impedance. Moreover, the concentrations of target molecules (e.g., hybridized miRNA-DNA) between TIEs could alter the capacitance between individual TIE electrodes. Similarly, the concentrations of non-target molecules (e.g., free complementary DNA and non-target miRNA) on TIEs could also alter the weak capacitance between electrodes that is produced by the leakage of electric fields through the air. First, we separately measured the impedance spectra (impedance vs. frequency) of 1 nM let-7b-miRNA, DNA complementary to let-7b, and hybridized let-7b-miRNA-DNA molecules (suspended in 0.01x TE buffer). Both DNA and miRNA have similar variations of phase spectra, but the miRNA-DNA molecules had a markedly different phase spectrum (Figure 3(g) yellow curve). These unique phase variations of single- (e.g., miRNA and DNA) and double-stranded (e.g., miRNA-DNA) molecules could be due to their structure (single- vs. double-stranded) and/or location within the TIEs (between vs. on TIEs).

To further understand the origin of the unique phase variation, we next performed another experiment in which we used a 10 Vpp electrical potential at 3 MHz to concentrate the molecules. Note that the single-stranded miRNA and DNA molecules experience larger dielectrophoretic forces at 3 MHz than the double-stranded miRNA-DNA molecules and concentrate between TIEs (Figure 3(a)). At 3 MHz, miRNA-DNA duplex molecules also experience a dielectrophoretic force and could also be concentrated between TIEs. For the phase spectra at 3 MHz, the miRNA, DNA, and miRNA-DNA molecules produced identical variations of the phase with frequency (Figure 3(h)). Moreover, note that the miRNA and DNA produced a variation pattern similar to that of the miRNA-DNA molecules at 1 MHz (Figure 3(g)). From these experimental evidences, it can be concluded

that the variation pattern of phase with frequency is more dependent on the locations of molecules within the device (between or on TIEs) than the molecules themselves. According to the phase vs. frequency data for miRNA-DNA duplex molecules concentrated between TIEs (Figure 3(g & h)), the phase spectrum can be sub-divided into low- and high-frequency regions. The low-frequency region lies between 1 Hz and 5 kHz (Figure 3(g & h)), in which the majority of the impedance is resistive $(-50° \leq \theta \leq -20°)$, and the high-frequency region lies between 5 kHz and 1000 kHz (Figure 3(g & h)), in which the impedance is reactive $(-90° \leq \theta \leq -50°)$. Similarly, for conjugated IL-6 antigen-antibody complexes suspended in 0.01x PBS, in the low-frequency (1 Hz-10 kHz) region, the impedance was resistive $(-40° \leq \theta \leq -10°)$ and in the high-frequency region (10 kHz – 1 MHz), the impedance was reactive $(-90° \leq \theta \leq -40°)$ (data not shown). We then investigated how impedance values measured in these regions correlate with molarities.

We used let 7b miRNA in experiments and performed all three steps of the detection and quantification assay stated above on the 0.01x TE buffer samples spiked with let-7b-miRNA molecules. Figure 4 shows the low-frequency (1 Hz-5 kHz) region and inset shows the high frequency region (5 kHz- 1MHz). Low–frequency impedance values could differentiate lower molarities (e.g., 1pM and 10 pM) better than high frequency impedance values. The impedance data show that limit of detection (LOD) and sensitivity of the sensor is highly dependent on the frequency. LOD provide the smallest level of biomarkers can be measured and sensitivity provides the gradient of the linear region (impedance vs. molarity). We were interested to study how different frequency regions contribute to LOD and sensitivity, which help to identify the frequency region appropriate for each biomarker type (e.g., miRNA or antigen). To simulate real world biomarker detection, we have conducted experiments to detect spiked molarities of miRNA and antigen in diluted serum samples.

We have used 1/10, 1/100 and 1/1000 as dilution factors but lower dilution factors, i.e., 1/10, cannot be used in our device because, at higher conductivity values, dielectrophoresis of molecules is not produced and/or the significantly higher temperatures produced in the solutions could disintegrate or degrade the biomolecules. Since the dilution factor of 1/100 is more relevant to real-world biomarker testing, we have discussed the sensor performance values of 1/100 to other sensing methods. We have slightly changed the frequency values

of low and high frequency range to improve the performance (LOD and sensitivity) and calculated the LOD and sensitivity values for let 7b-miRNA (Table 1(a)). Low frequency impedance produces better LOD (~fM) and high-frequency region provides high sensitivity for 1/100 diluted serum sample. In comparison, traditional impedance-sensing techniques have tedious assay steps including chemically attaching complementary DNA molecules on the glass substrate between interdigitated electrodes, hybridizing the target miRNA, producing miRNA-DNA duplexes, and measuring the impedance spectra, reported LOD values in the fM range.[39] In comparison, we have found low frequency produce fM LOD and high sensitivity for antigen molecules suspended in 1/100 diluted serum samples (Table 1(b)). It has been reported that the LOD of traditional ELISA is about 30 nM.[17] These evidences show that depending on the biomarker molecules, proper frequency region needed to select for measuring impedance values.

4. Concluding Remarks

We have demonstrated the proof-of-concept of a universal biosensing technology that could directly detect clinically relevant biomarker levels in diluted serum samples. In addition to miRNA and antigen biomarkers, universal biosensor could also be used to detect and quantify circulating short DNA molecules. Austin's group has previously demonstrated differential dielectrophoretic forces for double- and single-stranded long DNA molecules (> 1 kb) at low frequencies.[23] Therefore, long DNA molecules could also be detected by the proposed method. Generally, in clinical assays, it is necessary to detect single or multiple biomarkers (up to about 3–4 biomarkers) in a single assay.[1-5] To detect multiple biomarkers, the samples need to be divided into equal volumes and multiple devices could be used for each target. Since the assay cost is less than $50 (device fabrication: $15, complementary molecules and buffers: $35), the use of multiple devices/assays is not cost-prohibitive. The biomarker detection time is about 30 min or less, which includes 10 min for hybridization or conjugation, 10 min for the separation and concentration of target molecules, and 5–10 min for impedance measurements. Specificity of the sensing is controlled primarily by the target and complementary conjugation step (Step 1). Studies have reported that conjugation of a target biomarker with its complementary molecules can be optimized to significantly reduce the rate of false positives.[27] Sensitivity or LOD can further improve by

isolating antigen, miRNA and DNA biomarkers from serum suspending molecules in low-conductivity buffer (e.g., 0.01x TE), and perform the detection.

5. Acknowledgments

The authors thank Mr. Rounak Pokharel for helping with the impedance experiments. LV is grateful for the financial support from the NDSU doctoral dissertation fellowship. DN acknowledges the financial support from National Science Foundation CAREER grant (Award No: 1941748) and the Richard Offerdahl research grant. The authors thank the staff of the micro-fabrication facility at NDSU for their support in fabricating TIEs.

6. Conflict of Interest

Authors declare no conflict of interest.

References:

[1] M. Chicas, R. Roman, K. Sevedge, J. Kenna, A. Miller, L. Beaupre, J. Zubia, C. B. Smith, A. Pauls and T. Walczer. *Journal of Oncology Navigation & Survivorship*, **10**(11), pp. 454 (2019).

[2] D. Q. Chen, G. Cao, H. Chen, C. P. Argyopoulos, H. Yu, W. Su, L. Chen, D. C. Samuels, S. Zhuang, G. P. Bayliss and S. Zhao. *Nat. Commun.*, **10**(1), p.1476 (2019).

[3] A. Gençay Can, E. Ekşioğlu and F. A. Çakçı. *Lymphatic Res. Biol.*, 2019, **17**(3), p.368 (2019).

[4] H. Zetterberg and S. C. Burnham. *Mol. Brain*, **12**(1), p.26 (2019).

[5] E. O'Reilly, A. V. Tuzova, A. L. Walsh, N. M. Russell, O. O'Brien, S. Kelly, O. N. Dhomhnallain, L. DeBarra, C. M. Dale, R. Brugman and G. Clarke. *JCO Precision Oncology*, **3**, pp. 1(2019).

[6] M. Herreros-Villanueva, S. Duran-Sanchon, A. C. Martín, R. Pérez-Palacios, E. Vila-Navarro, M. Marcuello, M. Diaz-Centeno, J. Cubiella, M. S. Diez, L. Bujanda and A. Lanas. *Clin. Transl. Gastroenterol.*, **10**(1), p.1 (2019).

[7] Y. Niu, M. Su, Y. Wu, L. Fu, K. Kang, Q. Li, L. Li, G. Hui, F. Li and D. Gou. *Cancer Epidemiology and Prevention Biomarkers*, **28**(2), pp.327 (2019).

[8] A. Selvamani, D. Lewis, B. Lewis, M. J. Spohn and F. Sohrabji. *Stroke*, **50**(Suppl_1), pp.AWP196 (2019).

[9] M. R. Friedländer, W. Chen, C. Adamidi, J. Maaskola, R. Einspanier, S. Knespel and N. Rajewsky. *Nat. Biotechnol.*, **26**(4), p.407 (2008).

[10] F. Bettazzi, E. Hamid-Asl, C. L. Esposito, C. Quintavalle, N. Formisano, S. Laschi, S. Catuogno, M. Iaboni, G. Marrazza, M. Mascini and L. Cerchia. *Anal. Bioanal. Chem.*, **405**(2-3), pp.1025 (2013).

[11] L. Jiao, L. Zhang, W. Du, H. Li, D. Yang and C. Zhu. *Nanoscale*, **11**(18), pp.8798 (2019).

[12] B. Hayes, C. Murphy, A. Crawley, and R. O'Kennedy, *Diagnostics*, **8**(2), p.39 (2018).

[13] V. Gupta, I. Jafferji, M. Garza, V.O. Melnikova, D. K. Hasegawa, R. Pethig, and D.W. Davis, *Biomicrofluidics*, **6**(2), p.024133 (2012).

[14] S. Petralia, M. E. Castagna, E. Cappello, F. Puntoriero, E. Trovato, A. Gagliano, and S. Conoci, S., *Sensing and bio-sensing research*, **6**, pp.90-94 (2015).

[15] K. E. Sapsford, J. Francis, S. Sun, Y. Kostov, and A. Rasooly, *Analytical and bioanalytical chemistry*, **394**(2), pp.499-505 (2009).

[16] H. Zhang, H. Chang and P. Neuzil. *Micromachines*, **10**(6), p.423 (2019).

[17] L. Velmanickam, D. Laudenbach, & D. Nawarathna, *Physical Review E*, **94**(4), pp. 042408 (2016).

[18] B. H., Lapizco-Encinas, B. A., Simmons, E. B., Cummings, & Y. Fintschenko, *Analytical chemistry*, **76**(6), 1571-1579 (2004).

[19] H. J. Kim, H. Ahn, D. S. Lee, D. Park, J. H. Kim, J. Kim, D. S. Yoon and K. S. Hwang. *Sensors*, **19**(19), p.4152 (2019).

[20] Kikkeri, K., Kerr, B.A., Bertke, A.S., Strobl, J.S. and Agah, M.,*Journal of Separation Science*, *43*(8), pp.1576 (2020).

[21] R. J. Nelson, H. H. Hooper, A. K. Hauser, S. Singh, S. J. Williams and A. P. Sassi. U.S. Pat. 6,074,827, 2000.

[22] C. Acquah, Y. W. Chan, S. Pan, D. Agyei and C. C. Udenigwe. *J. Food Biochem.*, **43**(1), p.e12765 (2019).

[23] C. F. Chou, J. O. Tegenfeldt, O. Bakajin, S. S. Chan, E. C. Cox, N. Darnton, T. Duke and R. H. Austin. *Biophys. J.*, **83**(4), pp.2170(2002).

[24] S. Margalit, S. Avraham, T. Shahal, Y. Michaeli, N. Gilat, P. Magod, M. Caspi, S. Loewenstein, G. Lahat, D. Friedmann- Morvinski and R. Kariv. *Int. J. Cancer, 146(1):115 (*2019).

[25] V. Jayasooriya and D. Nawarathna. *Electroanalysis*, **29**(2), pp.330 (2017).

[26] G. Bhatt, K. Mishra, G. Ramanathan and S. Bhattacharya. *Sens. Actuators, B*, **288**, pp.442 (2019).

[27] L. Velmanickam, M. Bains, M. Fondakowski, G. P. Dorsam and D. Nawarathna. *J. Phys. D: Appl. Phys.*, **52**(5), p.055401 (2018).

[28] T. Akter, I. Atanelishvili, A. Noguchi, R. M. Silver and G. S. Bogatkevich. *PloS One*, **12**(11), p.e0188588 (2017).

[29] L. Seprödi, G. Biczo and J. Ladik. *Int. J. Quantum Chem.*, **3**(5), pp.621(1969).

[30] E. Chirshev, K. C. Oberg, Y. J. Ioffe, & J. J. Unternaehrer, *Clinical and Translational Medicine*, **8(1)**, 24 (2019).

[31] M.A.S. John, Y. Li, X. Zhou, P. Denny, C. M. Ho, C. Montemagno, W. Shi, F. Qi, B. Wu, U. Sinha and R. Jordan, *Archives of Otolaryngology–Head & Neck Surgery*, **130(8)**, pp.929-935 (2004).

[32] M. Reichl, M. Herzog, F. Greiss, M. Wolff and D. Braun. *Phys. Rev. E*, **91**(6), p.062709 (2015).

[33] N. G. Green, A. Ramos, A. Gonzalez, A., A. Castellanos, and H. Morgan, *Journal of Electrostatics*, *53*(2), pp.71-87 (2001).

[34] A. Castellanos, A. Ramos, A. Gonzalez, N. G. Green and H. Morgan, H., *Journal of Physics D: Applied Physics*, *36*(20), p.2584 (2003).

[35] G. Fuhr, T. Schnelle, and B. Wagner, *Journal of Micromechanics and Microengineering*, *4*(4), p.217 (1994).

[36] G. H. Markx, P.A. Dyda, and R. Pethig, *Journal of biotechnology*, *51*(2), pp.175-180 (1996).

[37] J. Wu, M. Lian, and K. Yang, *Applied physics letters*, ***90*(23)**, p.234103 (2007).

[38] L. Seprödi, G. Biczo, and J. Ladik, *International Journal of Quantum Chemistry***, 3(5),** pp.621-634 (1969).

[39] P. Jolly, M. R. Batistuti, A. Miodek, P. Zhurauski, M. Mulato, M.A. Lindsay, and P. Estrela. *Scientific reports*, 6, 36719 (2016).

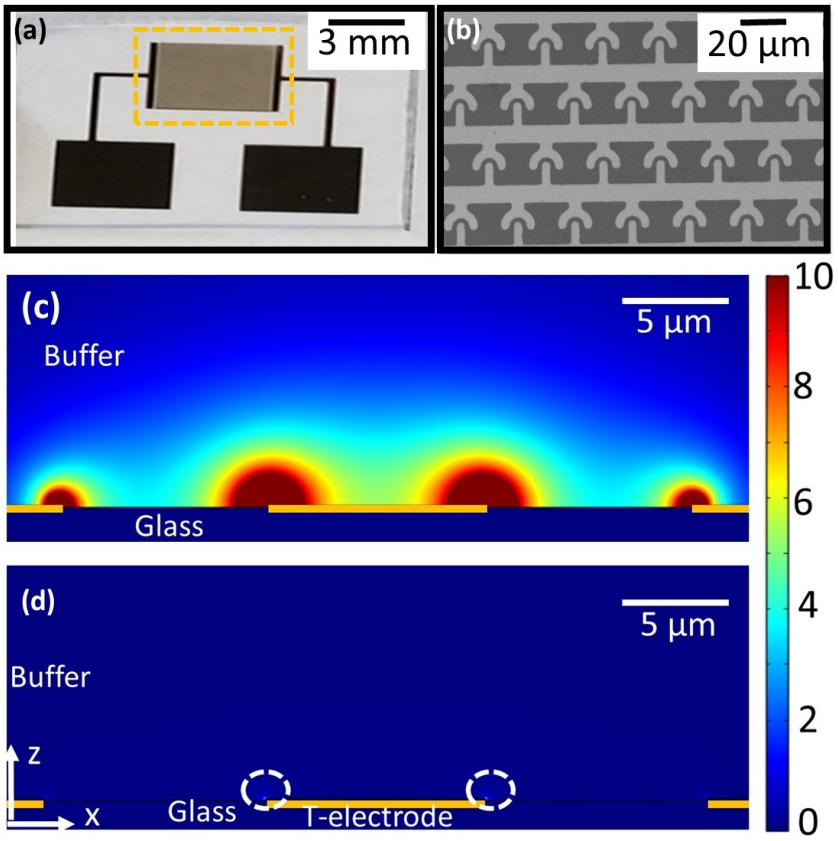

Figure 1: Universal biomarker sensing device and calculated dielectrophoretic capture volumes of target (miRNA-DNA duplex) and non-target (free miRNA or DNA) molecules. **(a)** A picture of the biosensor used in the experiments. The area enclosed in the yellow rectangle with broken line has an array of T-shaped interdigitated microelectrodes (TIEs). The sample was pipetted onto the TIEs for detection and quantification. **(b)** Scanning electron microscope image of TIEs that shows the shapes of individual electrodes and the density of TIEs. **(c, d)** Dielectrophoretic capture regions around the TIEs for miRNA-DNA (c) and DNA and miRNA molecules (d).

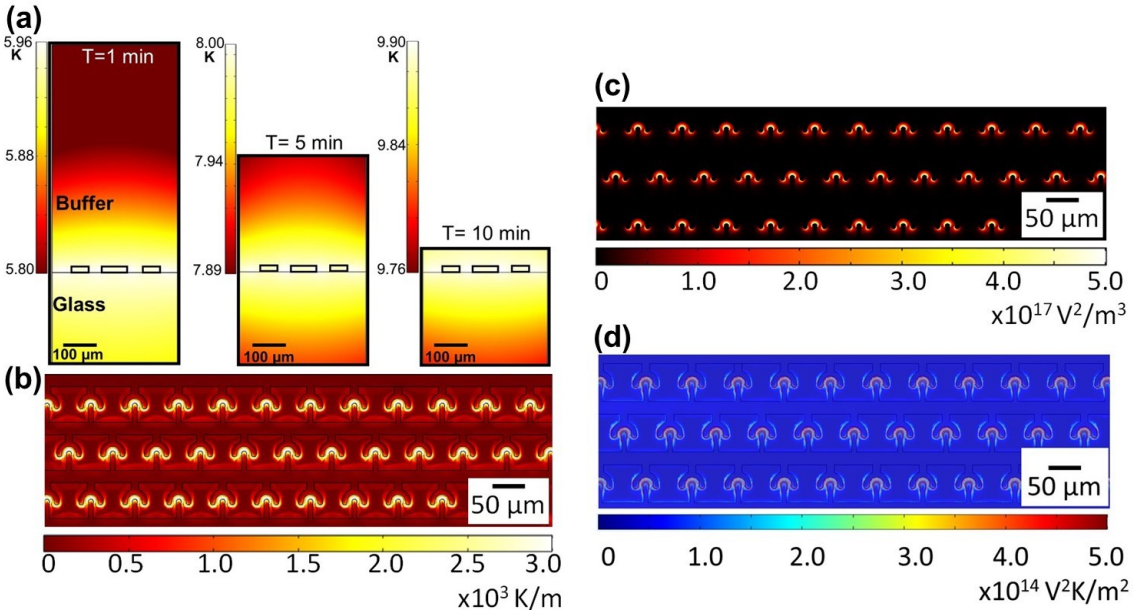

Figure 2: Conceptual demonstration of molecular separation and concentration between TIEs. **(a)** Calculated time- and distance-dependent (in x-z plane) temperature distribution (in Kelvin) around TIEs. Note that the sample volume gradually decreases with time, but locations of high- and low-temperature gradients do not change. **(b)** Calculated $\nabla(T)$ variation at x, y, z = 0 (or TIE plane). **(c)** Calculated $\nabla(E^2)$ variation at x, y, z = 0 (or TIE plane) **(d)** Variation of $E^2\nabla T$ at x, y and z=0 plane (TIE plane).

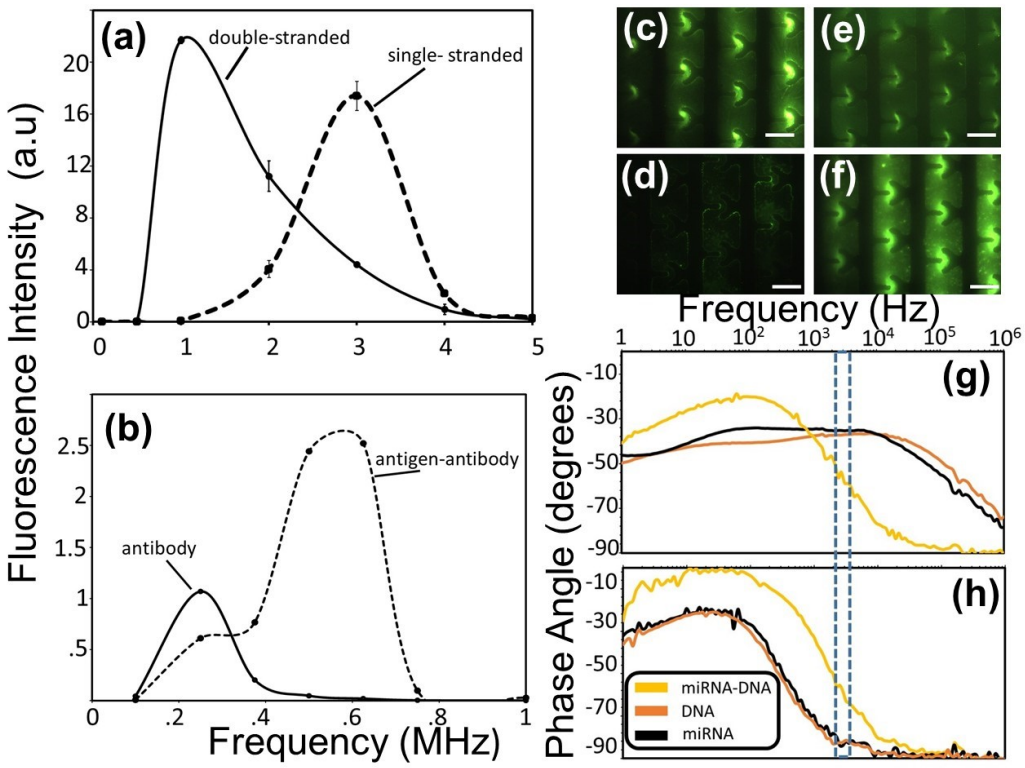

Figure 3: Experimental demonstration of the universal biosensing concept. **(a)** Variations in the fluorescence intensity (between TIEs) with the frequency of the applied electric potential for fluorophore-labeled let 7b-miRNA-DNA and single-stranded DNA that is complementary to let 7b miRNA. **(b)** Illustrates the fluorescence intensity vs. frequency for fluorophore-labeled conjugated IL-6 antigen-antibody complex and fluorophore-labeled IL-6 antibody molecules. **(c)** Fluorescence image of conjugated fluorophore (fluorescein) labeled IL-6 antigen-antibody (1μM) after applying 10 Vpp at 625 kHz for 10 min. **(d)** Fluorescence image of TIEs for conjugated fluorophore (fluorescein) labeled-DNA (1μM) after applying 10 Vpp at 1MHz for 10 min. **(e)** Fluorescence image recorded for fluorophore (fluorescein) labeled IL-6 antibody that underwent conditions stated in (c). **(f)** Fluorescence image recorded for complementary fluorophore (fluorescein) labeled miRNA-DNA that underwent conditions stated in (d). **(g & h)** Phase spectroscopy of miRNA-DNA (let-7b), miRNA (let-7b), and DNA molecules that complementary to let-7b at 1 MHz (g) and 3 MHz (h).

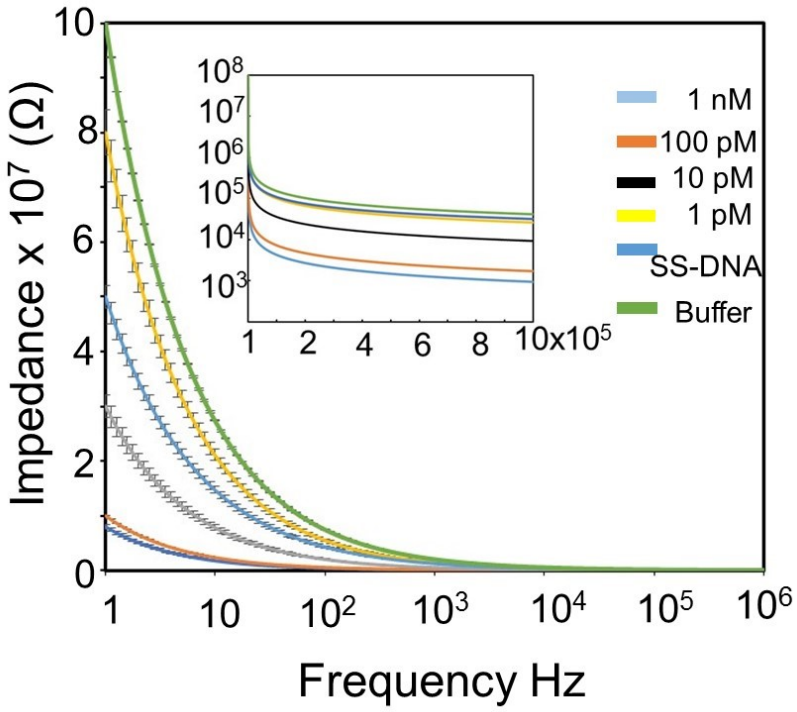

Figure 4: Analysis of impedance data from let 7b-miRNA-DNA and DNA that is complementary to let-7b (SS-DNA). The figure shows the impedance spectra from1 Hz to 1 MHz, and the inset shows the impedance spectra from .1 MHz to 1 MHz. Each experiment was repeated 2-3 times and average values and their standard deviations were calculated included in plots.

(a)

Frequency	Limit of Detection (LOD)		Sensitivity (Ω/M)	
	(1/100) Serum	(1/1000) Serum	(1/100) Serum	(1/1000) Serum
1 Hz- 1 KHz	84±4.3 fM	49±23 pM	(1.1±1)X 10^{15}	(3.1±1.7)X 10^{14}
1 KHz- 1 MHz	220±47 fM	79±52 fM	(4±2)X 10^{16}	(4.6±2.4)X 10^{12}

(b)

Frequency	Limit of Detection (LOD)		Sensitivity (Ω/M)	
	(1/100) Serum	(1/1000) Serum	(1/100) Serum	(1/1000) Serum
1 Hz- 100 Hz	75.44±45.9 fM	4.36±2.2 pM	(1.5±.7)X 10^{15}	(5.65±5.0)X 10^{16}
10 KHz- 1 MHz	6.09±4.3 pM	44.78±44.5 fM	(6.01±4.7)X 10^{13}	(2.62±2.2)X 10^{12}

Table 1: LOD and sensitivity values produced by the device in measuring spiked **(a)** miRNA (let-7b) and **(b)** antigen (IL-6) biomarkers directly in diluted serum samples.